Appl Phys B (2009) 95: 195–203
DOI 10.1007/s00340-009-3455-6

Applied Physics B
Lasers and Optics

The "arch" of simulating quantum spin systems with trapped ions

H. Schmitz · A. Friedenauer · C. Schneider · R. Matjeschk · M. Enderlein · T. Huber · J. Glueckert · D. Porras · T. Schaetz

Received: 17 October 2008 / Revised version: 4 February 2009 / Published online: 12 March 2009

Abstract We cannot translate quantum behavior arising with superposition states or entanglement efficiently into the classical language of conventional computers (Feynman et al. in Int. J. Theor. Phys. 21:467, 1982). A universal quantum computer could describe and help to understand complex quantum systems. But it is envisioned to become functional only within the next decade(s). A shortcut was proposed via simulating the quantum behavior of interest in another quantum system, where all relevant parameters and interactions can be controlled and observables of interest detected sufficiently well. For example simulating quantum spin systems within an architecture of trapped ions (Porras and Cirac in Phys. Rev. Lett. 92:207901, 2004). Here we specify how we simulate the spin and all necessary interactions and how we calibrate their amplitudes. For example via a two-ion phase-gate operation on two axial motional modes simultaneously at a fidelity exceeding 95%. We explain the complete mode of operation of a quantum simulator on the basis of our simple model case—the proof of principle experiment of simulating the transition of a quantum magnet from paramagnetic into entangled ferromagnetic order (Friedenauer et al. in Nat. Phys. 4:757, 2008) and emphasize some of the similarities and differences with a quantum computer.

PACS 03.67.Pp · 42.50.vk · 75.10.Jm · 77.80.Bh

H. Schmitz · A. Friedenauer · C. Schneider · R. Matjeschk · M. Enderlein · T. Huber · J. Glueckert · D. Porras · T. Schaetz (✉)
Max Planck Institute of Quantum Optics, Hans Kopfermann Str. 1, 85748 Garching, Germany
e-mail: tschaetz@mpq.mpg.de

1 Introduction

If we lack the possibility for direct calculation, we tend to step back and search for an analogue that might help to gain deeper understanding of our problem. One intriguing example was found by the British scientist Robert Hook [4] in 1675, not being capable to calculate the optimal form for maximal stability of masonry arches for building. His discovery was that the shape of a light flexible cord or chain subjected to specified loads would, when inverted, give the required shape of the perfect arch to carry those same loads. St. Paul's cathedral, for example, was build based on simulations within a model system of "one-dimensional" chains.

In our days, other interesting problems arise that are intrinsically impossible to be solved via classical calculus. For example simulations and the related deeper understanding of the dynamics of some tens of interacting quantum spins are intractable for the most powerful classical computers. The generic state of 40 spin-$\frac{1}{2}$ particles is defined by 2^{40} numbers and to describe its evolution a matrix of $2^{40} \times 2^{40}$ has to be exponentiated [5]. Even exponentially increasing classical calculation capabilities cannot help to efficiently simulate only slightly larger quantum systems. Already 300 particles require 2^{300} numbers describing the state, close to the estimated amount of protons in (one of) our universe(s).

As originally proposed by Richard Feynman [1], a quantum computer (QC) could efficiently simulate the dynamics of many-body quantum systems. A very promising candidate[1] might be based on trapped ions, suggested by Cirac and Zoller in 1995 [6].

However, translating the quantum dynamics of a system into an algorithm of stroboscopic gate operations and to run

[1] See, for instance, http://qist.lanl.gov/qcomp_map.shtml.

it on a potential universal quantum computer (capable to run arbitrary algorithms) requires the control of the order of 10^5 ions/quantum-bits (qubits) at operational fidelities $>99.99\%$ [7].

Even though there appear to be no fundamental obstacles for scaling the ion trap approach from six or eight ions/qubits in state of the art experiments [8, 9] at impressive operational fidelities of $>99\%$ [10], there is challenging technology to be developed.

To gain deeper insight into the dynamics of quantum systems, an alternative approach should be taken into consideration. We can choose a quantum system to be controlled and manipulated with its evolution governed by the same Hamiltonian as the system to be simulated. Porras and Cirac proposed in 2004 to simulate quantum spin Hamiltonians in ion traps adapting state of the art methods employed (developed) by the community working on quantum computation [2].

Already a chain of 40 ions/spins in a Paul trap should allow one to outperform any classical computer while slightly more in a two-dimensional grid would help to solve problems of actual interest (some theoreticians concerned with problems of solid-state physics see this in reach for two-dimensional systems of 10×10 to 20×20 ions/spins [11, 12]). This shortcut might be within reach at state of the art operational fidelities even if the quantum simulator (QS) gets affected by decoherence during its evolution. It might still allow for meaningful results (i.e. without involved quantum error correction) if one is interested in robust effects, like quantum phase transitions.[2]

It has to be noted, that a universal QC will have the capacity to run also arbitrary QS—not restricted to quantum spin systems only. And even within quantum spin systems, it will be able to address more questions, while the shortcut via QS at (right now) still lower operational fidelities will be restricted to investigate sufficiently robust effects. On the other hand, at comparable operational fidelities, QS might allow for even more efficient processing again, since they are intrinsically closer to the natural evolution [5]. Anyway, until a universal QC is available, different promising approaches for QS (e.g. within optical latices [13]) do not have to compete with each other, but their results might be combined to reconstruct enhanced insight.

The task of providing the feasibility test for QS involving several simulation ions/spins in an one-dimensional ion trap was achieved in our group recently [3]. In the following section, we try to introduce and briefly discuss the building blocks for generic quantum spin Hamiltonians.

[2] A uncorrected error in the running algorithm of a QC could already alter completely its output. However, state of the art operational fidelities might be sufficient for QS studying "fault-robust" effects while universal QC requires an enormous overhead of ancilla qubits to provide error correction (fault-tollerance).

However, there remains the fundamentally and technically important challenge to develop the ion-trap architecture that allows for scaling the simulator to a larger amount of ions/spins (100–400) and/or higher-dimensional systems.

2 Simulation of spin Hamiltonians

The Hamiltonians that can be realized with trapped ions can show Heisenberg like interaction [2, 14]. Quantum spin Hamiltonians of this type are supposed to describe many solid-state systems like magnets, high-T_c superconductors, quantum Hall ferromagnets, ferroelectrics etc., and their simulation would allow one to observe and analyze quantum phase transitions [2].

To implement QS-protocols for quantum spin Hamiltonians we have to realize the simulation of the spin, provide its initialization and final detection, the interaction of the spin with a magnetic field and the mutual spin–spin interaction.

In this section, we will try to explain the generic building blocks for the case of a linear chain of ions. The simplest and therefore the best system to investigate the feasibility of QS in ion traps is described by the quantum-Ising Hamiltonian,

$$H_{\text{Ising}} = H_J + H_B = J \sum_{m=n+1} \sigma_m^z \sigma_n^z - B_x \sum_m \sigma_m^x, \qquad (1)$$

requiring identical tools as the rest of the family of quantum spin Hamiltonians.

It consists of two contributions. The first part stands for the interaction between the spins of nearest neighbors in the 1D spin chain, represented by the Pauli matrices $\sigma_i^{x,z}$. The amplitude of J represents the interaction strength, while its positive (negative) sign stands for an anti-ferromagnetic (ferromagnetic) interaction. The latter part can be understood as the interaction of a magnetic field with each spin independently.

2.1 Simulating the spin

The mutual distance between the ions/spins aligned along the axis of the linear Paul trap is typically larger than 1 μm. Therefore, the interaction between their electronic (internal) states is negligible. In the following, we use the formal equivalence between a two-level system and a spin-$\frac{1}{2}$ magnetic moment in a magnetic field (Bloch-vector representation) [15, 16] to simulate the spin. The two-level system used at MPQ and depicted in Fig. 1 is spanned by the $|F = 3, M_F = -3\rangle$ and $|F = 2, M_F = -2\rangle$ ground-state hyperfine levels of $^{25}Mg^+$ labeled $|\downarrow\rangle$ and $|\uparrow\rangle$, respectively (splitting $\omega_0/2\pi = (E_\uparrow - E_\downarrow)/h \simeq 1.79$ GHz). The duration available for a simulation is in principle only limited by the decoherence of these internal states. The radiative lifetime of the hyperfine ground states is extremely long (many

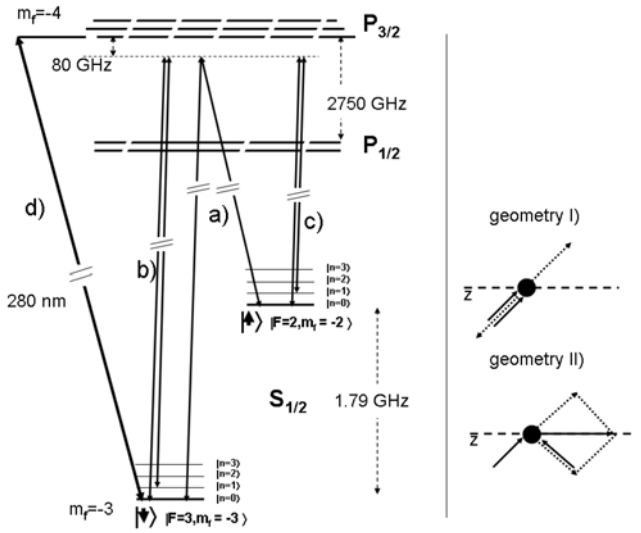

Fig. 1 On the *left hand side*: schematic of the relevant energy levels (not to scale) of one $^{25}Mg^{+}$ ion. Shown are the ground-state hyperfine levels providing the two internal states simulating the spin ($|\downarrow\rangle$ and $|\uparrow\rangle$) and the first three equidistant harmonic oscillator levels related to the harmonic axial confinement in a linear ion trap. Typically, the energy splitting of the motional levels and the Zeeman shift induced by a (real) external magnetic field are of the same order of magnitude within 1 to 10 MHz, therefore much smaller than the hyperfine splitting of 1.79 GHz, the fine structure splitting of 2750 GHz and the optical transition frequency of the order of 10^{15} Hz (280 nm). We depict the resonant transition for state sensitive detection named (**d**) and the relevant types of off resonant (by $2\pi \cdot 80$ GHz) two-photon stimulated Raman transitions. (**a**) The carrier transition coupling the internal states to simulate a magnetic field B_x. (**b**), (**c**) Realized by two beams to provide a state-dependent optical-dipole force simulating the spin–spin interaction J further described in the text. On the *right hand side* we depict the two different beam geometries for II (I) motionally (in)dependent transitions. The *solid arrows* represent the vectors $\vec{k}$ of the individual beams, the *dotted arrows* the recoils of the absorbed and emitted photons. For geometry I, the transferred momentum $\hbar|\Delta\vec{k}| \simeq 0$ while for geometry II $\hbar|\Delta\vec{k}| \simeq \sqrt{2}|\vec{k}|$ along the trap axis $\vec{z}$

years). Therefore, the memory decoherence is primarily due to phase errors induced by external perturbations, e.g. magnetic field fluctuations. In a carefully controlled environment decoherence timescales could be on the order of many days with experimentally demonstrated lower limits of several minutes (see e.g. [17]). For spin detection we distinguish the two states $|\downarrow\rangle$ and $|\uparrow\rangle$ by observing state-dependent laser driven fluorescence. The laser beam frequency is tuned to drive the spin from the $|\downarrow\rangle$ state to some exited state, as depicted in Fig. 1 via beam (d), which subsequently decays back to $|\downarrow\rangle$ emitting a photon that can be detected. When the spin is in the $|\downarrow\rangle$ state, the ion scatters many photons, approximately one per mille of them detected at a rate of the order of 10^5 Hz (see Fig. 4). For the spin in the $|\uparrow\rangle$ state, laser beam scattering is negligible [18].

The main advantage of simulating the spin is to circumvent the unavoidable "natural" interaction superimposed on the simulated ones. That is, the amplitude of the simulated

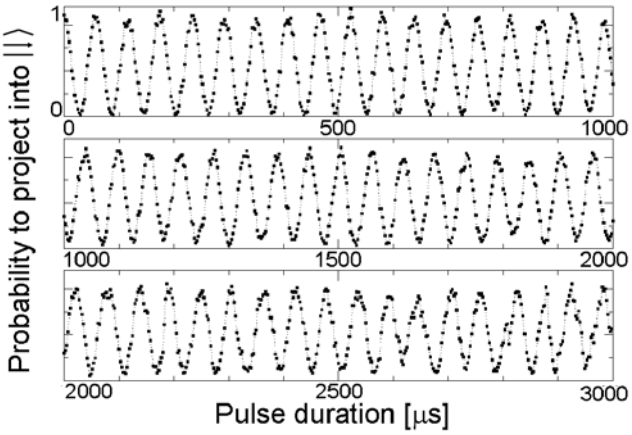

Fig. 2 Coherent oscillations of the spin. The probability to finally detect the spin in state $|\downarrow\rangle$ is depicted in dependence of the duration of the applied rf-field for up to 3000 μs. Driving transitions from the state $|\downarrow\rangle$ to the state $|\uparrow\rangle$ can be described as Rabi flopping on the Bloch sphere. Within the simulation, the rf-field provides the simulated magnetic field with its amplitude B_x being proportional to the inverse of the period of oscillation. Each data point represents the average of 500 measurements

interaction (and its range [2]) can be controlled and, for example, even completely switched off.

2.2 Simulating the magnetic field

We simulate an effective magnetic field by coupling the two electronic states $|\downarrow\rangle$ and $|\uparrow\rangle$ defined above via electromagnetic radiation. The coherent oscillation of the state population between the two levels is equivalent to Rabi flopping. In the description of the Bloch sphere picture the tip of the state vector rotates during one flop continuously on the surface from the state $|\downarrow\rangle$ to $|\uparrow\rangle$. For continued rotation this corresponds to the precession of a spin exposed to a perpendicular magnetic field.

We implement this coupling, in the following described by Ω_{Rabi}, either directly via a resonant radio-frequency (rf) field at $\omega_0/2\pi$ or indirectly via two-photon stimulated Raman transitions driven with two laser beams [19] depicted as (a) in Fig. 1. By tuning the difference frequency of the laser beams to $(\omega_1 - \omega_2)/2\pi = \omega_0/2\pi$, we implement rotations of the spin state,

$$R(\theta,\phi) \equiv \begin{pmatrix} \cos\frac{\theta}{2} & -ie^{-i\phi}\sin\frac{\theta}{2} \\ -ie^{+i\phi}\sin\frac{\theta}{2} & \cos\frac{\theta}{2} \end{pmatrix}, \tag{2}$$

where we use the conventions $|\downarrow\rangle \equiv (0,1)^T$, $|\uparrow\rangle \equiv (1,0)^T$. The angle θ is proportional to the duration t of the rf/Raman pulse ($\theta/2 = \Omega_{\text{Rabi}} \cdot t$). The phase factor ϕ is either defined by the rf-phase of the driving oscillator or $\phi = \Delta\vec{k} \cdot \vec{z} + \phi_1 - \phi_2$, the phase difference between the Raman beams at the position $\vec{z}$ of the ion ($\Delta\vec{k} \equiv \vec{k}_1 - \vec{k}_2$, the wave vector difference of the Raman beams). For the applications

via two laser beams we can use two different beam geometries, as depicted on the right hand side of Fig. 1. Here the beams are oriented in geometry I such that $\vec{k}_1$ is parallel to $\vec{k}_2$ ($|\Delta\vec{k}| \simeq 0$). Motion does not affect the transitions driven by these beams.

In any case, the relative phase ϕ defines a certain relative angle within the horizontal plane of the Bloch sphere identifying the axis of rotation for precessions. For example, if we apply a rotation $R(\pi/2, 0)$ on the ion and continue with a second identical rotation, we just flip the spin from $|\downarrow\rangle$ to $|\uparrow\rangle$ as if we applied a $R(\pi, 0)$ rotation around the same axis. But replacing the second operation by a rotation around an axis at 90 degrees relative to the first one via a $R(\pi/2, \pi/2)$, the effect of the second pulse can be interpreted as a rotation of the spin "around itself". The spin aligned with the new rotational axis is therefore not changing its state. For our simulation (see Sect. 3) this is equivalent to the spin being aligned with the magnetic field, an eigenstate of the system described by H_B (see (1)) that has to stay unchanged.

In Fig. 2 we depict typical data from a long term oscillation of the spin state (flopping curve) via the rf-radiation applied in our simulations. We measure the period for a 2π oscillation at a given rf-amplitude to calibrate the amplitude of our simulated magnetic field. We have

$$\frac{B_x \cdot t}{\hbar} = \frac{\theta}{2} = \Omega_{\text{Rabi}} \cdot t. \tag{3}$$

Applying the rf-amplitude provided during our simulation we determine a single spin rotation $R(2\pi, 0)$ within 118 µs and deduce $B_x/\hbar = 2\pi \cdot 4.24$ kHz.

2.3 Simulating the spin–spin interaction

To implement the interaction between different spins, the two Raman laser beams can be configured in a way that they cause state-dependent optical-dipole forces (see Fig. 1: the two Raman beams in geometry II coupling simultaneously (b) $|\downarrow\rangle \leftrightarrow P_{3/2}$ or (c) $|\uparrow\rangle \leftrightarrow P_{3/2}$).

The k-vectors of the beams are oriented such that $\vec{k}_1$ is approximately perpendicular to $\vec{k}_2$ and $\Delta\vec{k} \equiv \vec{k}_1 - \vec{k}_2 \simeq \sqrt{2}|\vec{k}_1|\vec{z} \equiv \vec{z}2\pi/\lambda_{\text{eff}}$, where λ_{eff} is the effective wavelength of the Raman beams. We choose the polarizations of the beams such that the different couplings due to the ac-Stark shifts by beams (b) or (c) and the associated forces are related by $\vec{F}_\downarrow = -3/2\vec{F}_\uparrow$ [20, 22]. They point along the trap axis $\vec{z}$ but in opposite directions.

This conditional interactions allows for the simulation of the spin–spin interaction [2]. To illustrate the idea, let us consider only one ion harmonically confined and exposed to a constant force. Searching for the quadratic complement leads to an identical but displaced harmonic oscillator potential. If we expose several ions, each individually confined and exposed to this force, all ions will be displaced to the new minima of their displaced harmonic potentials. If the force is dependent of the internal/spin state of each ion, we can receive additionally changes in the mutual distance of the displaced harmonic potentials. But now we have to consider additionally the (altered) Coulomb interaction between the ions. The term describing the Coulomb interaction between the ions in this new frame can be interpreted as the desired spin–spin interaction. This simplified explanation is illustrated in Fig. 3 for the case of two ions/spins. If both spins point into the same direction, the state-dependent optical-dipole force will push (or pull) the ions in common along the trap axis, therefore not changing the mutual distance and the Coulomb energy, respectively. But if the two spins point into opposite directions, one ion will be pulled while the other one will be pushed now changing their mutual distance. In the depicted scenario, the distance gets decreased, the Coulomb energy increased. This conditional attraction/repulsion can be interpreted as a spin–spin interaction.

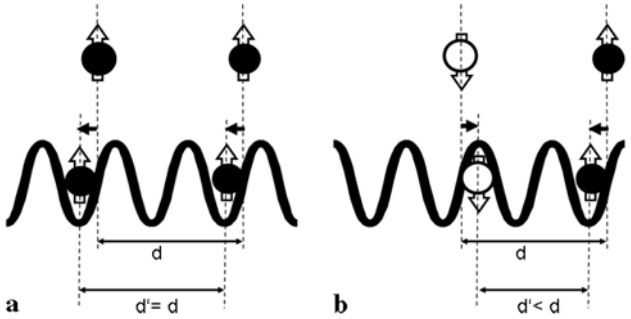

Fig. 3 Simplified illustration of the formation of the effective spin–spin interaction. We distinguish two scenarios with a mutual ion distance d equal to an integer amount of the effective wavelength λ_{eff} of the state-dependent optical-dipole force symbolized by the sinusoidal curve to guarantee that the ions/spins are exposed to the same phase of the force. The two ions in (**a**) are of identical internal state and are displaced in common by the interaction with the force: their distance d therefore remaining unchanged ($d' = d$). In (**b**) the two ions of different states get displaced relative to each other, changing the mutual distance $d' < d$. This conditional change in the ions distance can be interpreted as a spin–spin interaction mediated by the Coulomb energy (phonons) of the ion crystal

If nature gets to choose the ground state of this system, it will prefer the spins aligned, the ferromagnetic order.

Technical reasons forced us to alter the proposal of [2] from the state-dependent optical-dipole force induced by a standing- ($\omega_1 - \omega_2 = 0$) to a walking-wave approach ($\omega_1 - \omega_2 \neq 0$). On the one hand, the implementation of the standing wave requires a phase stabilization to compensate for fluctuations in the length of the different optical paths of the two beams to minimize spatial jitter of the pulsed wave. On the other hand, we would have to locate the ions/spins not only at a distance of an integer multiple of the effective wavelength but also at the position of the maximal gradient of the force.

Switching to the walking wave averages out the above described problem of phase jitter. It alters the static canonical transformation to one in the co-rotating (co-oscillating) frame with the displacement being time dependent. Within this new frame, the ions reside at rest again. Here, we can identify the motionally increased Coulomb energy summarized in a correction term as the spin–spin interaction H_J.

To calibrate the individual amplitudes for the spin–spin interaction by the applied fields in the QS separately (J without B_x), we implement a geometric phase gate [22] with two ions/qubits.

We first describe here a two qubit gate similar to the one in [22] using the stretch (out-of-phase) motional mode only to elucidate the basic idea. We adjust the frequency difference between the Raman beams and therefore the amplitude variation of the optical-dipole force to be equal to $\omega_2 - \omega_1 = \omega_{\mathrm{STR}} + \delta$. For $|\delta| \ll \omega_{\mathrm{STR}}$ we get $\omega_2 - \omega_1$ close to resonance of the out-of-phase motion of the ions at frequency $\omega_{\mathrm{stretch}} = \sqrt{3}\omega_{\mathrm{com}}$ (ω_{com} being the oscillation frequency of the in-phase or center-of-mass (com) motion). The ions are separated by a distance $m \cdot \lambda_{\mathrm{eff}}$ (were m is an integer) and therefore see the same phase of the state-dependent dipole force(s) as depicted in Fig. 3. We excite a relative motion of the ions (on the stretch mode) only for the states $|\downarrow\rangle|\uparrow\rangle$ and $|\uparrow\rangle|\downarrow\rangle$ (not for the states $|\downarrow\rangle|\downarrow\rangle$ and $|\uparrow\rangle|\uparrow\rangle$). If we excite the motion resonantly on the stretch mode ($\delta = 0$), we will continue enhancing the coherent motional excitation. By choosing the detuning $\delta \neq 0$, we accelerate the motion for the duration $|2\pi/\delta| \cdot 1/2$. When the force gets out of phase by more than π it decelerates the system returning it to its initial motional state after $|2\pi/\delta|$. We can describe this motion within phase space of the stretch mode as a circular path where the involved states pick up a geometric phase proportional to the phase-space area circumscribed.

This is equivalent to a geometric phase gate G_{ϕ_G}, which implements the operation [22]

$$\begin{aligned} G_{\phi_G} : {} & a|\downarrow\rangle|\downarrow\rangle + b|\downarrow\rangle|\uparrow\rangle + c|\uparrow\rangle|\downarrow\rangle + d|\uparrow\rangle|\uparrow\rangle \\ & \rightarrow a|\downarrow\rangle|\downarrow\rangle + e^{i\phi_G} b|\downarrow\rangle|\uparrow\rangle + e^{i\phi_G} c|\uparrow\rangle|\downarrow\rangle + d|\uparrow\rangle|\uparrow\rangle. \end{aligned} \quad (4)$$

The gate can be converted into a π-phase gate or a CNOT-gate in combination with single qubit rotations (as described in (2) and illustrated in Fig. 10), if we adjust the amplitude of the state-dependent optical-dipole force appropriately to achieve $\phi_G = \pi/2$. Starting, e.g. with the state $|\downarrow\downarrow\rangle$ and sandwiching this gate between two $R(\pi/2, 0)$ pulses in one arm of a spin-echo experiment (one additional $R(\pi, 0)$ pulse centered between the two other $R(\pi/2, 0)$ pulses) applied to both ions, we are able to produce maximally entangled states of the form $|\psi\rangle = |\downarrow\downarrow\rangle + |\uparrow\uparrow\rangle$ [22] as presented in Figs. 4 and 5.

We can describe this gate operation in terms of non-adiabatic spin–spin interaction to relate it to H_J in (1) to

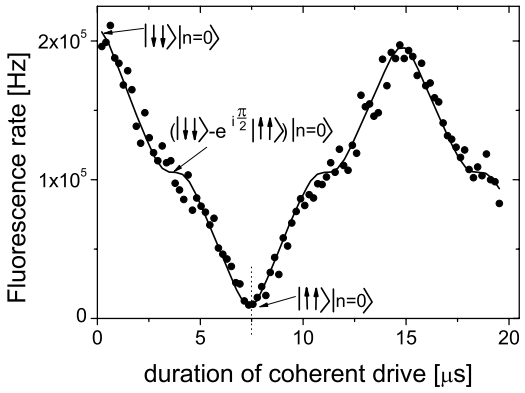

Fig. 4 Evolution of the initialized state $|\downarrow\downarrow\rangle|n = 0\rangle$ in dependence of the duration of the applied driving force. We embed the coherent motional excitation in a spin-echo experiment (see Fig. 10), as in [22]. The motional state returns here close to its ground state in the phase space of the stretch- and the com-mode after $T_G = 3.75$ μs and its multiples. Each time the theoretically expected curve (shown as *solid line*) flattens, we close the circles in phase space (one on the stretch and five on the com-mode) being equivalent to picking up a total differential phase of $\phi_G = \pi/2$. After 3.75 μs, we achieve approximately the state $(|\downarrow\downarrow\rangle - i|\uparrow\uparrow\rangle)|n = 0\rangle$ while after 15 μs the system returns close to state $|\downarrow\downarrow\rangle|n = 0\rangle$. The measured contrast in the detected fluorescence rate is in agreement with the independently determined fidelity of the gate operation exceeding 95%. Each data point represents the average of 500 measurements

calibrate J. Since the two sets of states acquire a geometric phase difference of $\pi/2$, we can deduce the related interaction amplitude J being proportional to the inverse of the required gate duration. We have

$$\begin{aligned} e^{i\frac{H_J}{\hbar}\cdot t}|\downarrow\rangle_1|\downarrow\rangle_2 &= e^{i\frac{J}{\hbar}\sigma_1^z\sigma_2^z\cdot t}|\downarrow\rangle_1|\downarrow\rangle_2 = e^{+i\frac{J}{\hbar}\cdot t}|\downarrow\rangle_1|\downarrow\rangle_2; \\ e^{i\frac{H_J}{\hbar}\cdot t}|\uparrow\rangle_1|\downarrow\rangle_2 &= e^{i\frac{J}{\hbar}\sigma_1^z\sigma_2^z\cdot t}|\uparrow\rangle_1|\downarrow\rangle_2 = e^{-i\frac{J}{\hbar}\cdot t}|\uparrow\rangle_1|\downarrow\rangle_2. \end{aligned} \quad (5)$$

To provide the phase-gate operation, the states $|\downarrow\rangle|\uparrow\rangle$ and $|\uparrow\rangle|\downarrow\rangle$ must pick up a phase difference of $\phi_G = \pi/2$ [22] after the duration T_G relative to the states $|\downarrow\rangle|\downarrow\rangle$ and $|\uparrow\rangle|\uparrow\rangle$. According to (5) this requires

$$2\frac{J}{\hbar}\cdot T_G = \frac{\pi}{2}. \quad (6)$$

To return to the motional ground state after the operation, the duration is chosen as $T_G = 2\pi/\delta$, providing

$$\frac{J}{\hbar} = \frac{\delta}{8}. \quad (7)$$

That is, we adjust the laser intensities I_1 and I_2 ($J \sim \Omega_{\mathrm{Rabi}}^2 \sim I_1 \cdot I_2$) [2] of the two beams providing the state-dependent optical-dipole force to turn a conditional circular path in phase space of one normal mode (e.g. the stretch mode) within T_G.

To realize the QS described in the next section or the related phase-gate operation we have to stay within the Lamb–Dicke regime. It requires us to keep the width of the mo-

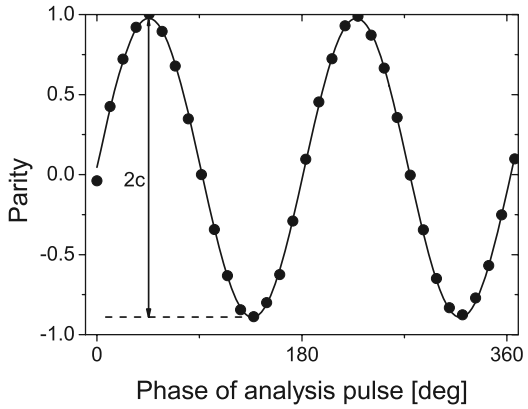

Fig. 5 Parity $(P_{\uparrow\uparrow} + P_{\downarrow\downarrow} - (P_{\uparrow\downarrow} + P_{\downarrow\uparrow}))$ after the duration of the coherent drive of 3.75 µs, providing an output close to the maximally entangled state $(|\downarrow\downarrow\rangle - i|\uparrow\uparrow\rangle)|n = 0\rangle$. Changing the phase of an additional analysis pulse $R(\pi/2, \phi_a)$ should oscillate the parity twice within ϕ_a out of [0; 360] degrees. The contrast $c/2$ of the best fit to the data indicated by the *solid line* provides information about the fidelity of the final entangled state preparation as mentioned in the caption of Fig. 4 and further described in [22]. Each data point represents the average of 1000 measurements

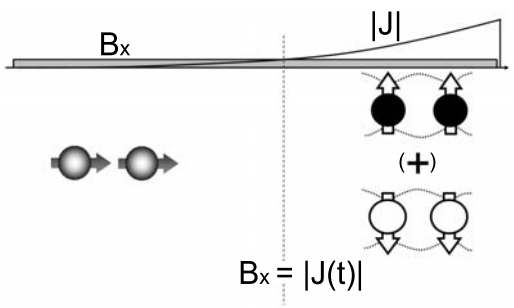

Fig. 6 Simplified illustration of the transition of two spins from paramagnetic into ferromagnetic order. We initialized the two spins in paramagnetic order $|\rightarrow\rightarrow\rangle$. Switching on the effective magnetic field parallel to the spin orientation does not affect the paramagnetic order, the ground state of the Hamiltonian H_B in (1). Increasing the effective spin–spin interaction adiabatically from 0 to $|J_{\max}| \gg B_x$ allows the spins to pass into the new ground state of the system (dominated by Hamiltonian H_J), the ferromagnetic order. Ideally, if the evolution does not get biased, we expect the system to undergo a symmetric transition into a superposition of the two ferromagnetic orders: a maximally entangled state of the type $(|\downarrow\downarrow\rangle + |\uparrow\uparrow\rangle)$

tional wave function small compared to the effective wavelength of the optical-dipole force to resolve its conditionality (phase) as illustrated in Fig. 3. The width of the motional wave function is in first order proportional to the average motional excitation $\bar{n}_z$, restricting its amplitude to $\bar{n}_z \simeq 1$.

After half the gate operation, the average motional excitation reaches its maximum at $\bar{n}_z = 1$ [22]. In addition, according to (7), the ratio of J/δ has to be kept constant. To allow for comparably large amplitudes of J necessary for the QS described in the next section, we have to pick a large detuning δ, since the chosen detuning $\delta_{\text{stretch}} = -2\pi \cdot 266$ kHz red from the stretch-mode frequency ω_{stretch} results in a detuning of $\delta_{\text{com}} = 2\pi \cdot 1330$ kHz blue of the com-mode frequency ($\omega_{\text{com}} = 2\pi \cdot 2.18$ MHz). The additional coupling is not negligible anymore. Due to the common motion (in phase) compared to the relative motion (out of phase) on the stretch mode, the direction of the loop is reversed. That is, the phase picked up in phase space of the stretch mode receives a relative minus sign. Choosing the detuning red of the stretch mode ($\delta_{\text{stretch}} < 0$) but blue of the com-mode ($\delta_{\text{com}} > 0$) compensates for this sign again and allows one to add the contributions of both modes constructively.

In addition, within the gate duration $T_G = 2\pi/\delta_{\text{stretch}}$, the system returns to the motional ground state of the stretch mode after one loop, but simultaneously to the motional ground state of the com-mode after five loops ($\delta_{\text{com}} = -5 \cdot \delta_{\text{stretch}}$).

Thus, the amplitude of the spin–spin interaction is composed by two contributions $J_{\text{sum}} = J_{\text{com}} + J_{\text{stretch}}$, the geometric phases gained within the two phase spaces have to add up again to $\phi_G = \pi/2$. Similar to (6) we obtain

$$2\frac{J_{\text{stretch}} + J_{\text{com}}}{\hbar} \cdot T_G = \frac{\pi}{2}, \tag{8}$$

with $T_G = 2\pi/\delta_{\text{stretch}}$ the duration for one loop in phase space of the stretch mode.

The experimental data presented in Figs. 4 and 5 allow to deduce a fidelity [22] exceeding 95% for achieving the maximally entangled state $(|\downarrow\downarrow\rangle - i|\uparrow\uparrow\rangle)$ after $T_G = 3.75$ µs, in good agreement with the theoretical expectations.

For the laser powers $P_{1,2}$ of 1.77 and 1.86 mW for the gate experiment (at beam waists $w_{1,2}$ of 30 µm and 36 µm) we deduce a related $J_{\text{sum}} = 2\pi \cdot 33$ kHz.

We use the determined J_{sum}, adapt it to the particular beam intensities ($I_{1,2} = 2P_{1,2}/(\pi w_{1,2}^2)$) to calibrate the amplitude of the spin–spin interaction in our QS. Fundamental differences of the quantum simulation and the gate operation of [22] are emphasized at the end of the experimental section.

3 Simulating the quantum magnet

The implementation of the experimental protocol for our feasibility study in the case of two spins is realized in the following way and is further described in [3] and illustrated in Fig. 6. (1) We prepare the two ions/spins close to the motional ground state ($\bar{n}_z \leq 0.03$) for both axial modes via Doppler- and subsequent sideband cooling and in the internal state $|\downarrow\downarrow\rangle$ via optical pumping. (2) We initialize both spins via a common $R(\pi/2, -\pi/2)$ rotation around the y-axis in the horizontal plane of the Bloch sphere (see (2)),

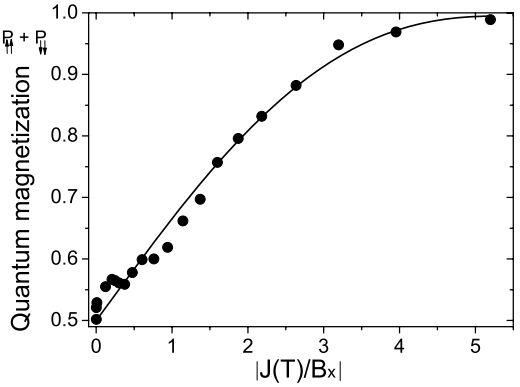

Fig. 7 Evolution of the initialized paramagnetic state $|\rightarrow\rightarrow\rangle = (|\downarrow\rangle + |\uparrow\rangle)(|\downarrow\rangle + |\uparrow\rangle) = (|\downarrow\downarrow\rangle + |\downarrow\uparrow\rangle + |\uparrow\downarrow\rangle + |\uparrow\uparrow\rangle)$ in dependence of the ratio of the amplitudes $|J(T)/B_x|$. The quantum magnetization is introduced as the probability to detect the ions/spins in the same state (ferromagnetic order). It increases to a final value of 98%, in agreement with the theoretical prediction depicted as *solid line*. Each data point represents the average of 1000 measurements

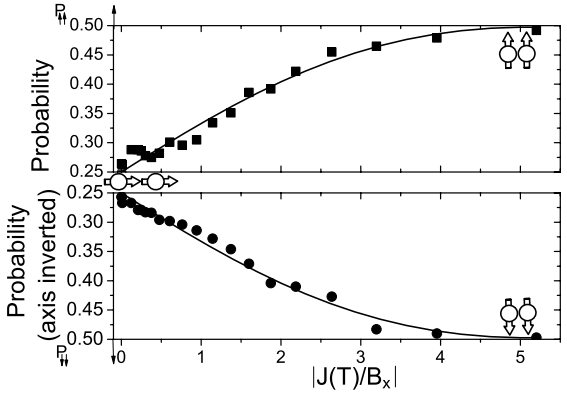

Fig. 8 Symmetric evolution of the initialized state $|\rightarrow\rightarrow\rangle$ in dependence of the ratio of the amplitudes of interactions $|J(T)/B_x|$ showing the probabilities $P_{\uparrow\uparrow}$ and $P_{\downarrow\downarrow}$ for the two ferromagnetic orders separately. The data of the symmetric evolution, i.e. for compensated bias fields. For comparison, we depict in Fig. 9 the evolution under influence of a dominating bias field. Each data point represents the average of 1000 measurements

aligned with its x-axis. (3) We switch on an effective magnetic field of amplitude B_x via coupling $R(2\pi, 0)$—not altering the initialized (eigen) state of the system. (4) We switch on adiabatically the effective spin-spin interaction J simulated by the state-dependent optical-dipole force provided by a walking-standing wave along the trap axis. (5) We read out the average state of the ions/spins.

For further analysis of the fidelity of entanglement in the final state we add to (4b) another analysis pulse $R(\pi/2, \phi_a)$ of variable phase ϕ_a, as for the data presented in Fig. 5 of the final state after the phase-gate operation.

Figure 7 depicts the probability to detect both spins in the same state after steps (1, 2, 3, 4, 5) of the protocol for the QS described above. Since the initialized state $|\rightarrow\rightarrow\rangle$ can be rewritten in our measurement basis (omitting normalization factors) as $(|\downarrow\rangle + |\uparrow\rangle)(|\downarrow\rangle + |\uparrow\rangle) = (|\downarrow\downarrow\rangle + |\downarrow\uparrow\rangle + |\uparrow\downarrow\rangle + |\uparrow\uparrow\rangle)$, we expect already a 50% probability $P_{\downarrow\downarrow} + P_{\uparrow\uparrow}$ to project this state in either $|\downarrow\downarrow\rangle$ or $|\uparrow\uparrow\rangle$. The invented quantum magnetization $M = P_{\downarrow\downarrow} + P_{\uparrow\uparrow}$ therefore starts at 0.5 for $J(T) \rightarrow 0$ after the duration of the simulation of $T = 120$ µs. For increasing final amplitudes of $J(T)$ to $J_{\max} = 2\pi \cdot 22$ kHz and the related ratio of $|J(T)/B_x| = 5.2$ we deduce a quantum magnetization of $M = 0.98$. For each presented data point, we repeat the simulation 500 times for identical parameters to gain the required statistics. In Fig. 8 we show the probabilities $P_{\uparrow\uparrow}$ and $P_{\downarrow\downarrow}$ separately. Minimizing all bias fields allows us to reveal the unbroken symmetry of the evolution.

In combination with the parity measurement (step (4b) in the protocol) we deduce a fidelity of the final entangled state of 88%.

For comparison we show the results for uncompensated (or additionally simulated) bias field B_z in Fig. 9. Its contribution is described via an additional term in (1), $H_{\text{Ising/bias}} = H_{\text{Ising}} + H_{\text{bias}}$ where $H_{\text{bias}} = B_z \sum_m \sigma_m^z$.

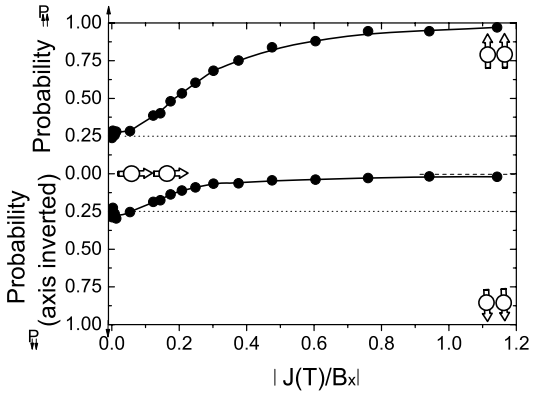

Fig. 9 Asymmetric evolution of the initialized state $|\rightarrow\rightarrow\rangle$ in dependence of the ratio of the amplitudes of interactions $|J/B_x|$ under the influence of a simulated bias field B_z. For bias fields, here related to stark shifts caused by the laser beams simulating the necessary interactions, we also obtain a final state with aligned spins. But this alignment is caused by the (simulated) external field and not due to a mutual spin-spin interaction. Therefore, the final orientation is biased by close to 100% into the direction of the simulated field. Each data point represents the average of 1000 measurements

To put the results of the simulation in the right perspective compared to the phase-gate operation, we have to emphasize their differences. Figure 10 illustrates the experimental protocols, with identical initialization and analysis fragments. The simulation itself consists of the interactions applied simultaneously including an adiabatic increase of J to transfer the system from the former ground state to the new one. Thus, if we extend the duration of the simulation the system will remain unchanged.

The phase-gate operation consists of independent stroboscopic pulses. The system does not reach a ground state and

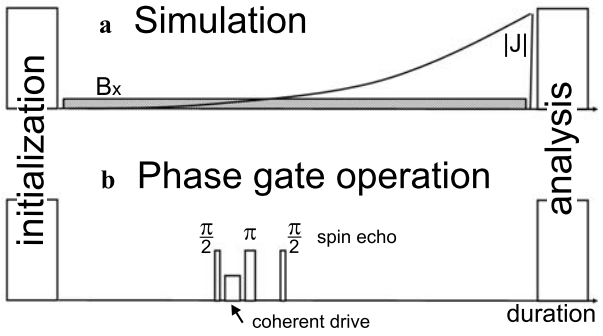

Fig. 10 Symbolized experimental protocols. The initialization and the analysis/detection can be described in equivalent terms. (**a**) The simulation requires both interactions, B_x and J, being applied simultaneously, with the amplitude of J increasing adiabatically. (**b**) The phase-gate operation is composed by a sequence of individual pulses, with the conditional coherent drive (which can be related to an isolated H_J) embedded in one arm of a spin-echo experiment

therefore oscillates. For continued gate operation, the system even returns to its initial state after $4 \cdot T_G$ as to be seen in Fig. 4.

On the one hand, it has to be noted that the same simulation can be performed principally on a large amount of ions/spins at the same time. This might emphasize the simplicity of the simulation in comparison to an increasing amount of stroboscopic gate operations. On the other hand, we have to mention that for an increased amount of spins the requirement of adiabaticity enforces longer simulation durations related to a longer exposure to decohering disturbances.

4 Conclusions and outlook

In the last few years the basic building blocks for a scalable architecture of a quantum information processor with trapped ion qubits have been demonstrated. Although it will be a nontrivial technological challenge to scale the system to many qubits, no fundamental limitations seem to exist. On a shorter timescale interesting problems might be studied by realizing an analog quantum simulator based on similar techniques, but with possibly less severe constraints on the fidelity of operations and the amount of required ions/spins. We demonstrated the proof of principle experiment that QS of spin-Hamiltonians can be performed with trapped ions.

We now aim to explore the limits of our feasibility study in the existing setup by e.g. increasing the amount of ions/spins in one dimension, investigating the influence of decoherence and adiabaticity to identify the challenges to be mastered for extending the simulations to larger quantum systems [23].

As the next step but to be faced in parallel, we will investigate the scalability of this approach to two-dimensional systems (within a feasibility study on two times two spins [23]). For this purpose, we will have to develop new micro fabricated cryogenic trapping structures.

Anyway, we hope to take advantage of the miniaturization and surface trap technology developed by the community of QC [21, 24], even though we are pushing towards a different objective: a real two-dimensional array of traps [23]. We plan to place linear surface ion traps close enough besides each other to provide stiff and controllable confinement of each ion individually, but to allow for sufficient Coulomb coupling (simulating e.g. spin–spin interaction) not only between ions confined in the same linear trap, but also between ions trapped in neighboring traps, close to a proposal of Cirac [25]. A cryogenic environment will be necessary to mitigate decohering effects due to the proximity to surfaces [26].

A comparably small amount of simulation spins, starting at approximately 10 times 10 ions/spins, might already allow one to address problems of interest in solid-state physics outperforming any future classical computer. For example investigating spin frustration suspected to be responsible for high temperature superconductivity [27].

In the mean time and to sharpen the experimental tools and knowledge and to emphasize the broad spectrum of physics to be addressed via QS, we should at least mention that there are several other proposals to be investigated. Simulating effects of relativity like the Dirac equation with one ion [28] or the production of squeezed states by non-adiabatically lowering the confining potential simulating the pair production of particles (here phonons within the ion crystal) in the early universe [29] or simulating the quantum random walk within an ion trap [30].

Acknowledgements The work described in this paper was supported by MPQ, MPG, DFG (Emmy-Noether Programme Grant No. SCHA 973/1-4), SCALA and by the DFG Cluster of Excellence Munich-Centre for Advanced Photonics. We thank Dave Wineland and Dietrich Leibfried for their invaluable altruistic input for the field of trapped ions in general and especially, discussions and knowledge sharing with our group. Ignacio Cirac, Gerhard Rempe and Rainer Blatt for their great intellectual and financial support.

References

1. R.P. Feynman, Int. J. Theor. Phys. **21**, 467 (1982)
2. D. Porras, J.I. Cirac, Phys. Rev. Lett. **92**, 207901 (2004)
3. A. Friedenauer, H. Schmitz, J. Glueckert, D. Porras, T. Schaetz, Nat. Phys. **4**, 757 (2008)
4. R. Hooke, A Description of Helioscopes, and Some Other Instruments (London, 1675)
5. S. Lloyd, Science **273**, 1073 (1996)

6. J.I. Cirac, P. Zoller, Phys. Rev. Lett. **74**, 4091 (1995)
7. M.A. Nielsen, I.L. Chuang, *Quantum Computation and Quantum Information*, 1st edn. (Cambridge University Press, Cambridge, 2000)
8. D. Leibfried, E. Knill, S. Seidelin, J. Britton, R.B. Blakestad, J. Chiaverini, D.B. Hume, W.M. Itano, J.D. Jost, C. Langer, R. Ozeri, R. Reichle, D.J. Wineland, Nature **438**, 639 (2005)
9. H. Haeffner, W. Hänsel, C.F. Roos, J. Benhelm, D. Chek-al-kar, M. Chwalla, T. Körber, U.D. Rapol, M. Riebe, P.O. Schmidt, C. Becher, O. Gühne, W. Dür, R. Blatt, Nature **438**, 643 (2005)
10. J. Benhelm, Nat. Phys. **4**, 463 (2008)
11. D. Feder, Private communication (2007)
12. J.I. Cirac, Private communication (2006)
13. D. Porras, J.I. Cirac, Phys. Rev. Lett. **93**, 263602 (2004)
14. E. Jané, G. Vidal, W. Dür, P. Zoller, J.I. Cirac, quant-ph/0207011 (2002)
15. R.P. Feynman, F.L. Vernon, R.W. Hellwarth, J. Appl. Phys. **28**, 49 (1957)
16. L. Allen, J.H. Eberly, *Optical Resonance and Two-Level Atoms* (Dover, Mineola, 1987)
17. J. Bollinger, D.J. Heinzen, W.M. Itano, S.L. Gilbert, D.J. Wineland, IEEE Trans. Instrum. Meas. **40**, 126 (1991)
18. R. Blatt, P. Zoller, Eur. J. Phys. **9**, 250 (1988)
19. D.J. Wineland, C. Monroe, W.M. Itano, D. Leibfried, B. King, D.M. Meekhof, J. Res. Natl. Inst. Stand. Technol. **103**, 259 (1998)
20. D.J. Wineland, M. Barrett, J. Britton, J. Chiaverini, B. DeMarco, W.M. Itano, C. Langer, D. Leibfried, V. Meyer, T. Rosenband, T. Schätz, Philos. Trans. R. Soc. Lond. A **361**, 1349 (2003)
21. J. Chiaverini, Quantum Inf. Comput. **5**, 419 (2005)
22. D. Leibfried B. DeMarco, V. Meyer, D. Lucas, M. Barrett, J. Britton, W.M. Itano, Nature **422**, 412 (2003)
23. T. Schaetz, A. Friedenauer, H. Schmitz, L. Petersen, S. Kahra, J. Mod. Opt. **54**, 2317 (2007)
24. S. Seidelin, J. Chiaverini, R. Reichle, J.J. Bollinger, D. Leibfried, J. Britton, J.H. Wesenberg, R.B. Blakestad, R.J. Epstein, D.B. Hume, W.M. Itano, J.D. Jost, C. Langer, R. Ozeri, N. Shiga, D.J. Wineland, Phys. Rev. Lett. **96**, 253003 (2006)
25. J.I. Cirac, P. Zoller, Nature **404**, 579 (2000)
26. J. Labaziewicz, Y. Ge, P. Antohi, D. Leibrandt, K.R. Brown, I.L. Chuang, Phys. Rev. Lett. **100**, 013001 (2008)
27. P.W. Anderson, Science **235**, 1196 (1987)
28. L. Lamata, J. Leon, T. Schaetz, E. Solano, Phys. Rev. Lett. **98**, 253005 (2007)
29. R. Schuetzhold, M. Uhlmann, L. Petersen, A. Friedenauer, H. Schmitz, T. Schaetz, Phys. Rev. Lett. **99**, 201301 (2007)
30. B.C. Travaglione, G.J. Milburn, Phys. Rev. A **65**, 032310 (2002)